Edge imaging characteristics of aberrated coherent optical systems by edge masking of circular apertures

M. Venkanna [1], K. D. Sagar [2]
[1] BVRIT Hyderabad College of Engineering for Women, Hyderabad, India;
[2] Optics Research Group, Department of Physics, Osmania University, Hyderabad, India

Abstract

In this paper, attempts have been made to study the joint effects of apodization and aperture masking on the diffraction images of coherently illuminated straight edge. The Edge-Ringing, Edge-Shift and Edge-Eradient of the edge images have been evaluated for different values of apodization using edge masking of circular apertures. We have considered rotationally symmetric, aberrated coherent optical system. These investigations have lead to the use of certain pupil functions in conjunction with optimal apodizers to assess the quality of edge images. Any obstruction placed in the light path of an optical system prevents waves from a portion of the wavefront in reaching the focal zone. This results in the change in the light flux at every point of the diffraction pattern. This is in turn, depends on the shape and size of the obstruction.

Keywords: amplitude filters, apodization, coherence, defocus, edge image, edge masking, primary spherical aberrations.

Citation: Venkanna M, Sagar KD. Edge imaging characteristics of aberrated coherent optical systems by edge masking of circular apertures. Computer Optics 2022; 46(3): 388-394. DOI: 10.18287/2412-6179-CO-940.

Introduction

Apodization can be accomplished in several ways i.e., by altering the shape of the aperture or its transmission characteristics [1]. The former is known as "Aperture Shaping" in which the shape and size of the aperture is altered. The later is known as "Aperture Shading" by using a spatial filter over the pupil from point to point (Mondal and Venkat Reddy, 1987). Thus apodization is the process of changing the energy distribution in the point spread function by deliberate manipulation of the pupil function so as to improve some measure of the image quality [2]. Apodization in optics is similar to pulse shaping in electrical engineering [3, 4]. Straubel may be considered as the founder of apodization theory [5]. When the amplitude transmittance of the pupil is gradually decreased from the center to edge of the pupil, the higher spatial frequencies are reduced and this manifests as suppression of side lobes. Apodization is one aspect of the more encompassing technique of "spatial filtering" (Hecht and Zajac, 1987). Apodization is useful in improving selected aspects of the imaging performance of an aberrated optical system [6 – 9]. Several researchers have studied the edge-ringing and edge-shifting properties of different pupil functions with a motivation to improve the quality of images [10 – 12]. The edge ringing is the difference between the first maximum intensity of the edge fringes and the unit object intensity. Edge-shift, which is also called the image shift, is the distance of the image edge at half of the intensity value of the object edge. Edge-gradient is the increase in image intensity over an unit change in Z around the geometric edge (i.e., $Z = 0$). It is desirable to design a system which would yield real and positive amplitude impulse to avoid the edge-ringing in coherent and partially coherent illuminations. This problem has been investigated and shown that the edge ringing is controllable by suitable apodizers [13]. Aperture shaping mitigates the deleterious effects of edge ringing in coherent imagery in the absence and presence of aberrations. The distinguishing feature of coherent optical system is the existence of a sharp cut-off of the transfer function. An edge object has strong high frequency components. The cut-off of the coherent optical system is effectively at a low value as compared to Fourier spectrum of the sharp edge and physical result is the unwanted edge ringing [14].

Apodization can be used for various purposes, in particular, for suppression of optical side-lobes in the diffraction field of an optical imaging system [15 – 16], for increasing depth of field [17 – 21] and also to enhance resolution [22 – 27]. The efficiency of apodization technique is always associated with the design of the pupil function. It is known that apodization in order to reduce the size of the focal spot of the point spread function (PSF) often leads to the growth of side lobes. Therefore, various approaches to finding a compromise solution are considered [28 – 32].

The presence of these spurious fringes in the edge response and the apparent shift of the imaged edge, cause the location and the measurement of the edge, difficult. Studies on this subject indicate the importance of coherent imagery in areas like spatial filtering techniques and microscopy.

Theory and formulation

An opaque straight edge is one which is bright on one side of a line and dark on the other. The mathematical

form of amplitude transmission of an opaque straight edge object [33] is given by

$$\begin{aligned} A(u,\ v) &= 1 \quad for\ u \geq 0, \\ A(u,\ v) &= 0 \quad for\ u < 0. \end{aligned} \tag{1}$$

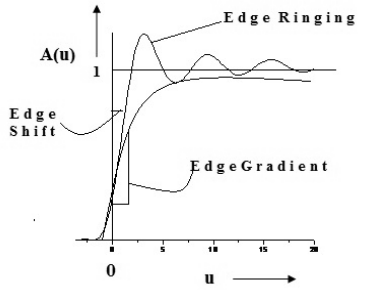

Fig. 1. Edge response

It is evident that A(u) is non-converging. Therefore, it does not permit Fourier transformation directly. However, this difficulty can be overcome by expressing it in terms of "signum" function as

$$A(u) = \frac{1}{2}\left[1 + Sgn(u)\right].$$

Where $Sgn(u)$ is defined as

$$\begin{aligned} Sgn(u) &= 1\ for\ u \geq 0, \\ Sgn(u) &= -1\ for\ u < 0. \end{aligned} \tag{2}$$

A sequence of transformable functions which approach $Sgn(u)$ as a limit should be considered, as this function also has a discontinuity at $u = 0$.
For example, the function

$$f(u) = \left[\exp\left(-\sigma|u|\right) Sgn(u)\right] \to Sgn(u)\ \ as\ \ \sigma \to 0. \tag{3}$$

Hence the Fourier transform of equation (3) will be

$$\begin{aligned} &F.T.\left[f(u)\right] = \\ &= \int_{-\infty}^{\infty} \exp\left(-\sigma|u|\right) Sgn(u) \exp\left(-2i\pi u x\right) du = \\ &= \int_{-\infty}^{0} -\exp\left[\left(\sigma - i2\pi x\right)u\right] du + \\ &+ \int_{0}^{\infty} \exp\left[\left(-\sigma + i2\pi x\right)u\right] du = \\ &= -\frac{1}{\left(\sigma - i2\pi x\right)} + \frac{1}{\left(\sigma + i2\pi x\right)}. \end{aligned} \tag{4}$$

As $\sigma \to 0$, the above expression equals to $(1/i\pi x)$ i.e.,

$$F.T[f(u)] = \exp\left[\left(-\sigma|u|\right) Sgn(u)\right] = \frac{1}{i\pi x}.$$

Thus expressing the straight edge in terms of $Sgn(u)$ as given in (2) and its Fourier transform can be obtained as

$$\begin{aligned} &F.T.\left[A(u,v)\right] = F.T.\left[\frac{1}{2}\left\{1 + Sgn(u)\right\}\right] = \\ &= \int_{-\infty}^{\infty} \left[1 + \left(-\sigma|u|Sgn(u)\right)\right] \exp\left(-i2\pi u x\right) dx = \\ &= \frac{1}{2}\left[\delta(x) + \frac{1}{i\pi x}\right]. \end{aligned} \tag{5}$$

Where, $\delta(x)$ is the well–known Dirac-delta function. The expression (5) gives the Fourier spectrum of the object amplitude distribution defined by (1). In this spectrum, the presence of a large zero frequency impulse at $x = 0$ is observed, in addition to the other non-zero frequency components. Looking at the object function in fig (1), it appears at the first sight that $A(u, v)$ is purely zero frequency input to the optical system and therefore, the presence of those non-zero frequencies in the spectrum of such an object may appear rather strange. It should be, however, observed that the object function has zero transmission over one-half in its own plane and a transmission equal to unity over the other half. In other words, $A(u, v)$ is zero for $u < 0$ and then there is an abrupt discontinuity at $u = 0$. Thus, $A(u, v)$ is not a true D.C. signal as it is not constant over the entire interval ranging from $-\infty$ to ∞ and this explains the presence of the other frequency components in the spectrum.

The imaging positions, encountered in optics are generally concerned with objects where amplitude or intensity variations are to be considered in two dimensions. The complex object amplitude distribution as defined in equation (1) implies that there is no variation in amplitude transmission of the object along the entire y-direction. This will give rise to an infinite impulse at $y = 0$ in the spectrum plane and can be represented by the Dirac-delta function $\delta(y)$. Finally, therefore, the two-dimensional F.T. of the object function is obtained as

$$a(x,y) = \frac{1}{2}\left[\delta(x) + \frac{1}{i\pi x}\right]\delta(y). \tag{6}$$

The above expression gives the spectrum of the object amplitude distribution $A(u, v)$ at the entrance pupil of the optical system. The modified object amplitude spectrum at the exit pupil of the optical system will be given by

$$a'(x,y) = a(x,y).T(x,y). \tag{7}$$

Where $T(x, y)$ is the pupil function of the given optical system having aberrations can be expressed [33] as

$$T(x,y) = f(x,y)\exp[i\varphi(x,y)]. \tag{8}$$

Where $f(x, y)$ denotes the amplitude transmittance over the pupil and $\varphi(x, y)$ indicates the wave aberration function of the optical system. In the absence of apodisation, $f(x, y)$ is taken to be equal to unity i.e., for the Airy pupils, $f(x, y) = 1$.

For defocus and primary spherical aberrations, the aberration function can be expressed as

$$\varphi(x,y) = \left[-\left(\frac{1}{2}\varphi_d r^2 + \frac{1}{4}\varphi_s r^4 \right) \right].$$

Here φ_d - defocus coefficient, φ_s - primary spherical aberration coefficient and is the normalized distance of an arbitrary point on the pupil from its centre.

$$r = \sqrt{x^2 + y^2}\,.$$

From expressions (6), (7) and (8) the modified amplitude spectrum at the exit pupil is given by

$$a'(x,y) = \frac{1}{2}\left[\delta(x) + \frac{1}{i\pi x} \right] \delta(y) f(x,y) \exp[i\varphi(x,y)]. \quad (9)$$

The above equation (9) gives the modified spectrum of the object at the exit pupil of the system. The complex amplitude distribution in the image plane will be given by the inverse F.T. of (9). Therefore,

$$\begin{aligned} A'(u',v') &= \frac{1}{2}\int_{-\infty}^{+\infty}\int \left[\delta(x) + \frac{1}{i\pi x} \right] \times \\ &\times \delta(y) f(x,y) \exp\left[i\varphi(x,y) \right] \times \\ &\times \exp\left[2\pi i (u'x + v'y) \right] dx\,dy. \end{aligned} \quad (10)$$

The integration limits of equation (10) are only formal because the pupil function given by $T(x,y)$ vanishes outside the pupil and can be assumed to be unity inside. Thus, after some manipulation in the integration of Eq. (10) by employing the filtering property of Dirac-delta function the expression (10) can be simplified as

$$\begin{aligned} A'(u',v') &= \frac{1}{2} f(0,0) \exp(i\varphi(0,0)) + \\ &+ \frac{1}{2\pi}\int_{-1}^{1} f(x,0) \frac{\cos(\varphi(x,0) + 2\pi u'x)}{x} dx - \\ &- \frac{i}{2\pi}\int_{-1}^{1} f(x,0) \frac{\cos(\varphi(x,0) + 2\pi u'x)}{x} dx. \end{aligned} \quad (11)$$

The filtering property of Dirac-delta function is represented by

$$\int_{-\infty}^{+\infty} \delta(x) f(x)\, dx = f(0). \quad (12)$$

For the central transmittance of the pupil function $f(0) = 1$, then the expression (11) can be expressed as

$$\begin{aligned} A'(u',v') &= \frac{1}{2} + \frac{1}{2\pi}\int_{-1}^{1} f(x,0) \times \\ &\times \exp\left[i\varphi(x,0) \right] \frac{\sin(2\pi u'x)}{x} dx - \\ &- \frac{i}{2\pi}\int_{-1}^{1} f(x,0) \exp\left[i\varphi(x,0) \right] \frac{\sin(2\pi u'x)}{x} dx. \end{aligned} \quad (13)$$

For the rotationally symmetric pupil function

$$f(x,y) = f(-x,-y).$$

Setting $2\pi u' = Z$ in equation (13), then it reduces to the more explicit formula for the image of an edge object.

$$A'(Z) = \frac{1}{2} + \frac{1}{2\pi}\int_{-1}^{1} f(x,0) \exp\left[i\varphi(x,0) \right] \frac{\sin(Zx)}{x} dx. \quad (14)$$

Further simplification leads to

$$A'(Z) = \frac{1}{2} + \frac{1}{\pi}\int_{0}^{1} f(x,y) \exp\left[i\varphi(x,0) \right] \frac{\{\sin(Zx)\}}{x} dx. \quad (15)$$

The present work deals with the one-dimensional straight edge object and hence, the general form of amplitude distribution is given by

$$A'(Z) = \frac{1}{2} + \frac{1}{\pi}\int_{0}^{1} f(x,0) \exp\left[i\varphi(x,0) \right] \frac{\{\sin(Zx)\}}{x} dx. \quad (16)$$

Pupil function $f(r)$ for the Hanning amplitude filter is given by

$$f(r) = \cos^2(\pi\beta r).$$

Here β is the apodization parameter. The term β controls the degree of non-uniformity of transmission over the pupil. A value of $\beta = 0$, corresponds to diffraction limited airy system having uniform transmission of unity over the entire aperture.

For the given aperture apodized with the Hanning amplitude filter in the presence of defocus and primary spherical aberration the expression (16) becomes

$$\begin{aligned} A'(Z) &= \frac{1}{2} + \frac{1}{\pi}\int_{0}^{\varepsilon} \mathrm{Cos}^2(\pi\beta r) \times \\ &\times \exp[-i(\varphi_d \frac{x^2}{2} + \varphi_s \frac{x^4}{4})] \frac{\sin(Zx)}{x} dx. \end{aligned} \quad (17)$$

Here $0 < \varepsilon \le 1$ is the edge masking parameter.

The intensity distribution of an edge image formed by an apodized optical system is given by the squared modulus of expression (17)

$$B(Z) = |A'|^2. \quad (18)$$

Results and discussion

The investigations on the effects of aperture masking on the images of edge objects formed by coherent optical systems apodized by the Hanning amplitude filter in the presence of defocus and primary spherical aberrations have been evaluated using the expressions (18) by employing Matlab simulation. The intensity distribution $B(Z)$ in the images of straight edge objects has been obtained for different values of dimensionless diffraction variable Z varying from – 3 to + 20.

The image quality assessment parameter such as Edge-Ringing (ER), Edge-Shift (ES) and Edge-Gradient (EG) have been studied for various values of apodization, aberrations and aperture edge masking parameter. The edge masking parameter of the aperture considered is

$\varepsilon = 1$, 0.9, 0.8, 0.7, 0.6 and 0.5. However the value $\varepsilon = 1$ represents the case of circular aperture.

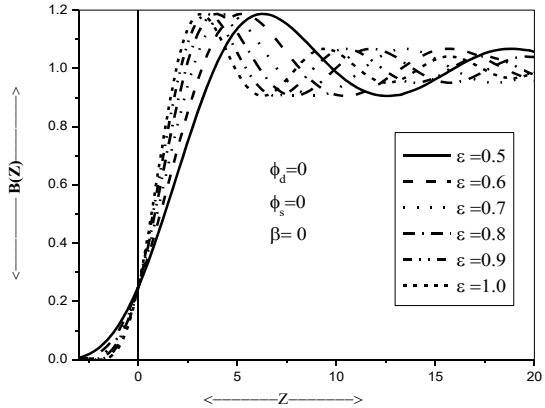

Fig. 2. Unapodized edge image intensity distributions by aberration-free and edge masked aperture

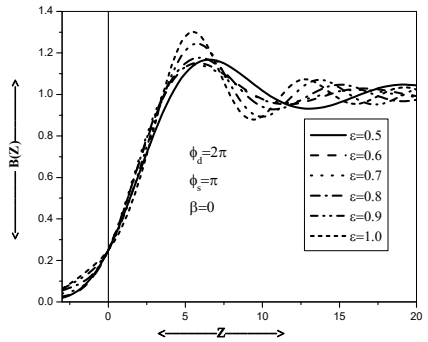

Fig. 3. Unapodized edge image intensity distributions by aberrated and edge masked aperture

Fig. 2 shows the intensity distribution profile of the straight edge for unapodized and aberration free optical system (Airy case) for both the circular and the edge masked apertures. The edge ringing is pronounced and is insensitive to edge masking parameter ε as the system is unapodized. Fig. 3 illustrates the case where the apodization parameter is $\beta = 0$ when $\varphi_d = \pi$ and $\varphi_s = 2\pi$. For the un-masked aperture, the negative maximum amplitude increases and hence the presence of ringing is much more pronounced.

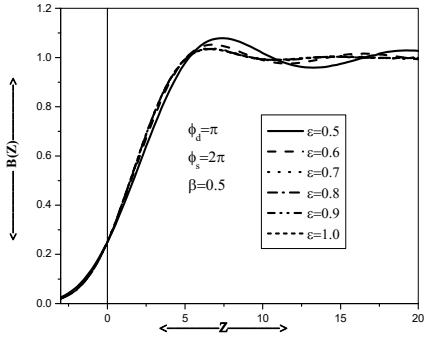

Fig. 4. Apodized edge image intensity distributions by aberrated and edge masked aperture

However, by increasing the masking zone of the circular aperture, the unwanted edge ringing has been reduced along with the edge shift at the cost of decrease in the edge gradient as the system is unapodized. From the fig. 4 it is observed that, at the apodization parameter $\beta = 0.5$, by increasing the masking zone of the aperture, i.e., from $\varepsilon = 1$ to 0.7, the unwanted edge ringing and edge shift have been reduced and an improvement in the edge gradient.

Figures from 5 to 7 depict the intensity distribution of edge images when the coherent optical system is at the defocused plane $\varphi_d = 2\pi$ in the presence of primary spherical aberration and apodized by the Hanning amplitude filter. We found that, increase in edge ringing with edge masking parameter ε for $\varphi_d = \pi/2$ and π planes, but it decreases along with increase in edge gradient at $\varphi_d = 3\pi/2$, 2π in the presence of apodization. Hence these defocused planes may be designated as the optimal receiving image planes to reduce the effect of primary spherical aberrations. It is evident that the apodized optical systems are more sensitive to aperture edge masking than the unapodized ones. The effect of primary spherical aberration is also studied and seen that, at certain defocused planes, i.e., at $\varphi_d = 2\pi$, aperture edge masking lowering the ringing effect even in the absence of aperture shading and it is more effective with the aperture shading. From the intensity distribution profiles, it is evident that, Hanning amplitude filter is very helpful in suppressing the ringing effect even in the presence of primary spherical aberration and defocus at $\beta = 0.5$. It is also fine for aperture masking as there is little variation of the skimming of light (ringing-effect) for various values of ε with the apodization.

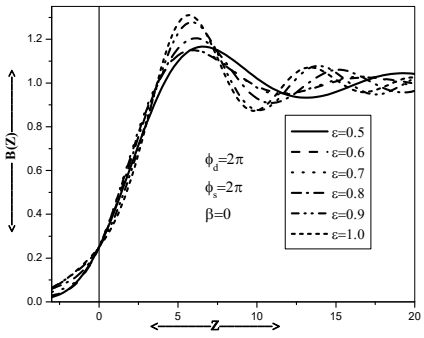

Fig. 5. Unapodized edge image intensity distributions by aberrated and edge masked aperture

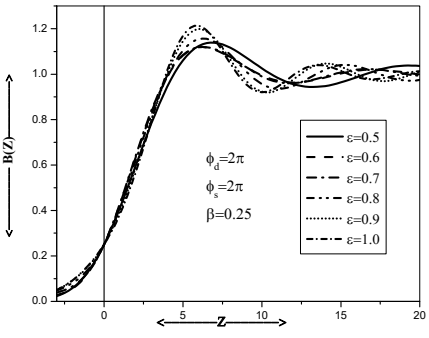

Fig. 6. Apodized edge image intensity distributions by aberrated and edge masked apertures

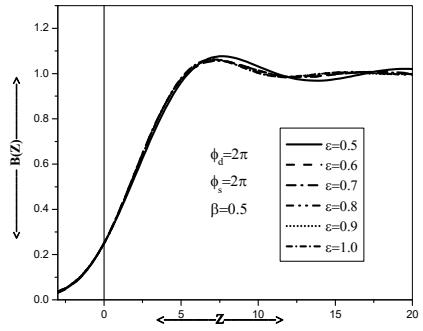

Fig. 7. Apodized edge image intensity distributions by aberrated and edge masked apertures

Fig. 8 shows the variation of the edge- ringing with the aperture edge masking parameter ε for different defocused planes in the presence of primary spherical aberration with and without apodization.

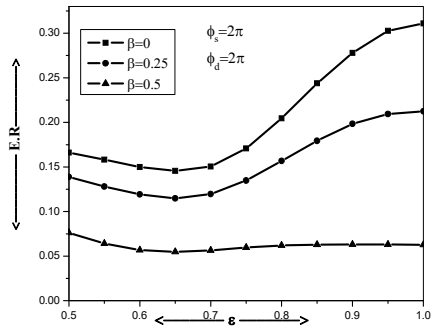

Fig. 8. Variation of Edge Ringing with ε

The magnitude of edge-ringing is found to be almost constant for all the values of ε as the system is aberration-free and unapodized, i.e., for Airy pupil. For the planes $\varphi_d = \pi/2$ and π, the edge-ringing is increasing with ε but it is in decreasing trend for $\varphi_d = 3\pi/2$ and 2π and attains the minimum (0.13946) value at ε = 0.7 for $\varphi_d = 2\pi$, when β=0.5. The similar features are observed for various degree of primary spherical aberration. For these values the edge-ringing is almost the same. The edge-ringing is much more pronounced with ε varies from 1 to 0.7 for the defocused planes$\varphi_d = 0$, $\pi/2$ and π. But it attains much lower value for $\varphi_d = 3\pi/$ and 2π at ε = 0.7.

Fig. 9 depicts the edge gradient curves for $\varphi_s = 2\pi$ and $\varphi_d = 2\pi$ for apodization values β = 0, 0.25 and 0.5. The value of edge gradient for the clear circular aperture (ε = 1) is lower when compared to that of the masked aperture. Clearly, there is an increase in the edge gradient (E.G) with ε decreasing. Even for high values of defocus and primary spherical aberration, it is evident that there is an improvement in the edge gradient with ε decreasing from 1 to 0.65 for β ≤ 0.5.

The variation in the edge shift has been presented for different values of ε in fig. 10 when the optical system apodized with β = 0, 0.25and 0.5 in the presence of both defocus and primary spherical aberration. It is observed that with ε varying from 1 to 0.5, the edge shift increases for $\varphi_d = \pi$ and $\varphi_s = 2\pi$ when the system is un-apodized but it is in decreasing trend when the system is apodized .

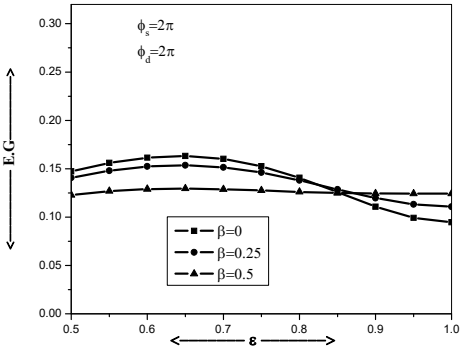

Fig. 9. Variation of Edge Gradient with ε

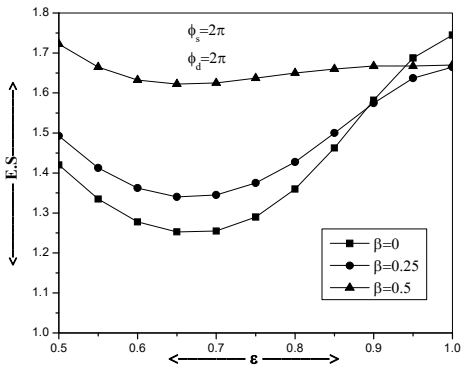

Fig.10. Variation of Edge Shift with ε

However, edge shift is the minimum at ε = 0.7 when $\varphi_d = 2\pi$ and $\varphi_s = \pi$ and at ε = 0.65 when $\varphi_d = 2\pi$ and $\varphi_s = 2\pi$. For these planes the edge shift shows a remarkable decrease in its value, which in turn enhances the edge gradient.

Tab. 1provides the computed values of edge ringing, edge gradient, edge shift and the product of edge gradient and edge shift for various values of apodization parameter β, edge masking parameter ε and different degrees of primary spherical aberration when the optical system is studied at various focal planes. It is seen that with edge masking parameter ε the edge ringing decreases with defocus. However, the edge ringing is less for clear circular aperture when compared to that of masked one in the absence of apodization. For β = 0.5 the decrease in edge ringing is almost 56.6 % when $\varphi_d = \pi$. This reduction in the edge ringing is almost 56.4 % when $\varphi_s = \varphi_d = \pi$ and ε = 0.5. When $\varphi_s = \varphi_d = 2\pi$ and ε = 0.65, the decrease in edge ringing is about 62.3 % when the optical system is apodized with β = 0.5. The product of ES and EG is almost constant for β = 0.5.

*Tab. 1 Variation of ER, EG, ES and EG*ES with ε for β = 0, 0.25 and 0.50*

	β	ε	ER	EG	ES	EG*ES
		0.50	0.1809	0.1557	1.3550	0.2109
		0.55	0.1784	0.1695	1.2425	0.2106
		0.60	0.1746	0.1824	1.1525	0.2103
		0.65	0.1705	0.1940	1.0800	0.2096
		0.70	0.1653	0.2040	1.0225	0.2086
	0	0.75	0.1592	0.2118	0.9800	0.2076
		0.80	0.1530	0.2170	0.9500	0.2062
		0.85	0.1493	0.2191	0.9350	0.2049
		0.90	0.1500	0.2177	0.9300	0.2025
		0.95	0.1596	0.2125	0.9425	0.2002
		1.00	0.1785	0.2034	0.9700	0.1973
		0.50	0.1504	0.1481	1.4275	0.2114
		0.55	0.1425	0.1597	1.3225	0.2112
		0.60	0.1334	0.1702	1.2375	0.2106
$\varphi_d=\pi$		0.65	0.1245	0.1792	1.1725	0.2101
		0.70	0.1154	0.1866	1.1250	0.2099
	0.25	0.75	0.1073	0.1922	1.0875	0.2090
$\varphi_s=\pi$		0.80	0.1007	0.1957	1.0650	0.2084
		0.85	0.0974	0.1970	1.0525	0.2074
		0.90	0.0984	0.1962	1.0500	0.2060
		0.95	0.1044	0.1933	1.0600	0.2049
		1.00	0.1146	0.1886	1.0775	0.2032
		0.50	0.0788	0.1280	1.6600	0.2125
		0.55	0.0644	0.1344	1.5825	0.2127
		0.60	0.0514	0.1394	1.5275	0.2129
		0.65	0.0411	0.1429	1.4875	0.2126
		0.70	0.0344	0.1453	1.4625	0.2125
	0.50	0.75	0.0299	0.1467	1.4500	0.2127
		0.80	0.0283	0.1473	1.4425	0.2125
		0.85	0.0280	0.1475	1.4400	0.2124
		0.90	0.0279	0.1475	1.4400	0.2124
		0.95	0.0281	0.1474	1.4400	0.2123
		1.00	0.0281	0.1474	1.4400	0.2123
		0.50	0.1662	0.1474	1.4200	0.2093
		0.55	0.1583	0.1560	1.3350	0.2083
		0.60	0.1499	0.1616	1.2775	0.2064
		0.65	0.1456	0.1632	1.2525	0.2044
		0.70	0.1505	0.1602	1.2550	0.2011
	0	0.75	0.1708	0.1526	1.2900	0.1968
		0.80	0.2045	0.1407	1.3600	0.1913
		0.85	0.2438	0.1259	1.4625	0.1841
		0.90	0.2779	0.1109	1.5825	0.1755
		0.95	0.3028	0.0993	1.6875	0.1675
		1.00	0.3111	0.0948	1.7450	0.1654
		0.50	0.1388	0.1407	1.4925	0.2100
		0.55	0.1282	0.1480	1.4125	0.2090
		0.60	0.1194	0.1524	1.3625	0.2077
$\varphi_d=2\pi$		0.65	0.1148	0.1537	1.3400	0.2060
		0.70	0.1196	0.1515	1.3450	0.2040
	0.25	0.75	0.1348	0.1461	1.3750	0.2009
$\varphi_s=2\pi$		0.80	0.1568	0.1381	1.4275	0.1971
		0.85	0.1794	0.1287	1.5000	0.1931
		0.90	0.1984	0.1198	1.5750	0.1886
		0.95	0.2095	0.1133	1.6375	0.1854
		1.00	0.2124	0.1109	1.6650	0.1846
		0.50	0.0762	0.1229	1.7225	0.2116
		0.55	0.0642	0.1269	1.6650	0.2112
		0.60	0.0568	0.1290	1.6325	0.2106
		0.65	0.0548	0.1295	1.6225	0.2101
		0.70	0.0563	0.1288	1.6250	0.2093
	0.50	0.75	0.0597	0.1275	1.6375	0.2088
		0.80	0.0620	0.1261	1.6500	0.2080
		0.85	0.0629	0.1250	1.6600	0.2075
		0.90	0.0631	0.1244	1.6675	0.2075
		0.95	0.0631	0.1243	1.6675	0.2072
		1.00	0.0628	0.1243	1.6700	0.2075

Conclusions

The important conclusions of the investigations on the effects of aperture masking on the images of straight edge objects formed by the coherent aberrated optical system apodized with the amplitude filters are summarized as: All the maxima on the bright side depend on the amount of masking zone of the aperture. It means edge images can be restored by decreasing the band pass region of the aperture. The un-apodized optical systems are less sensitive to the aperture masking in the absence of defocus than the apodized ones. The unwanted edge ringing is found to reduce even at defocused planes with the aperture edge masking.

Apodization along with aperture masking is useful in improving the performance of defocused coherent optical systems. For $\varphi_d=2\pi$ the edge ringing shows a decreasing trend and there is an improvement in edge gradient for both unapodized and apodized optical systems with edge masking of the aperture. Hence at this defocused plane the optical system can be considered to be optimum in edge imaging. By edge masking of the aperture, we can reduce the diffraction effects and improve contrast. This technique in the telescopes reduces the image blurring effects of atmospheric turbulence and sharpening the image.

References

[1] Hecht E, Zajac A. Optics. 2nd ed. Addison-Wesley, USA; 1978: 422, 496, 497, 512.

[2] Wetherell WB. The calculation of image quality parameters. In Book: Shannon RR, Wyant JC, eds. Applied optics and optical engineering. Vol 8. Ch 6. New York: Academic press; 1980: 173-283.

[3] Papoulis A. Maximum intensity of diffraction patterns and apodization. J Opt Soc Am 1967; 57(3): 362-366. DOI: 10.1364/JOSA.57.000362.

[4] Papoulis A. Systems and transforms with applications in optics. McGraw-Hill Book Company; 1968: 442.

[5] Rao KP, Mondal PK, Seshagiri Rao, T. Coherent imagery of straight edges with Straubel apodisation filters. Optik 1978; 50: 73-81.

[6] Barakat R. Solution of the luneberg apodization problems. J Opt Soc Am 1962; 52(3): 264-275. DOI: 10.1364/JOSA.52.000264.

[7] Mills JP, Thompson BJ. Effect of aberrations and apodization on the performance of coherent optical systems. II. Imaging. J Opt Soc Am A 1986; 3(5): 704-716.

[8] Venkanna M, Karuna Sagar D. Reduction in edge-ringing in aberrated images of coherent edge objects by multishaded aperture. Advances in Optics 2014; 2014: 963980. DOI: 10.1155/2014/963980.

[9] Venkanna M, Karuna Sagar D. Amplitude filters in shaping the point spread function of optical imaging systems. Proc SPIE 2015; 9654: 96540A. DOI: 10.1117/12.2181610.

[10] Katti PK, Gupta BN. Effect of amplitude filter on the partially space coherent diffraction of a defocused optical system. J Opt Soc Am 1972; 62(1): 41-44

[11] Tschunko HFA. Apodization and image contrast. Appl Opt 1979; 18(7): 955-956.

[12] Araki T, Asakura T. Coherent apodization problems. Opt Commun 1997; 20(3): 373-377.

[13] Leaver FG, Smith RW. Use of apodization in coherent imaging systems. Optik 1973, 39: 156-160.

[14] Considine PS. Effects of coherence on imaging systems. J Opt Soc Am 1966; 56(8): 1001-1009. DOI: 10.1364/JOSA.56.001001.
[15] Jacquinot P, Roizen-Dossier B. II Apodization. Prog Opt 1964; 3: 29-186. DOI: 10.1016/S0079-6638(08)70570-5.
[16] Siu GG, Cheng L, Chiu DS. Improved side-lobe suppression in asymmetric apodization. J Phys D: Appl Phys 1994; 27(3): 459-463. DOI: 10.1088/0022-3727/27/3/005.
[17] Dowski ER, Cathey WT. Extended depth of field through wavefront coding. Appl Opt 1995; 34(11): 1859-1866. DOI: 10.1364/AO.34.001859.
[18] Pan C, Chen J, Zhang R, Zhuang S. The extension ratio of depth of field by wavefront coding method. Opt Express 2008; 16(17): 13364-13371. DOI: 10.1364/OE.16.013364.
[19] Khonina SN, Ustinov AV. Generalized apodization of an incoherent imaging system aimed for extending the depth of focus. Pattern Recognit Image Anal 2015; 25(4): 626-631. DOI: 10.1134/S1054661815040100.
[20] Dzyuba A, Serafimovich P, Khonina S, Popov S. Application of a neural network for calculating the surface relief of a different level two-zone lens with an increased depth of field. Proc SPIE 2020; 11516: 115161A. DOI: 10.1117/12.2565993.
[21] Khonina SN, Volotovskiy SG, Dzyuba AP, Serafimovich PG, Popov SB, Butt MA. Power phase apodization study on compensation defocusing and chromatic aberration in the imaging system. Electronics 2021; 10(11): 1327. DOI: 10.3390/electronics10111327.
[22] Barakat R. Application of apodization to increase two-point resolution by Sparrow criterion under incoherent illumination. J Opt Soc Am 1962; 52(3): 276-283. DOI: 10.1364/JOSA.52.000276.
[23] Kowalczyk M, Zapata-Rodriguez CJ, Martinez-Corral M. Asymmetric apodization in confocal scanning systems. Appl Opt 1998; 37(35): 8206-8214.
[24] Khonina SN, Ustinov AV. Sharper focal spot for a radially polarized beam using ring aperture with phase jump. J Eng 2013; 2013: 512971. DOI: 10.1155/2013/512971.
[25] Reddy ANK, Sagar DK, Khonina SN. Complex pupil masks for aberrated imaging of closely spaced objects. Opt Spectrosc 2017; 123(6): 940-949. DOI: 10.1134/S0030400X17120189.
[26] Reddy ANK, Khonina SN. Apodization for improving the two-point resolution of coherent optical systems with defect of focus. Appl Phys B 2018; 124(12): 229. DOI: 10.1007/s00340-018-7101-z.
[27] Reddy ANK, Hashemi M, Khonina SN. Apodization of two-dimensional pupils with aberrations. Pramana 2018; 90(6): 77. DOI: 10.1007/s12043-018-1566-5.
[28] Hopkins HH, Zalar B. Aberration tolerances based on line spread function. J Mod Opt 1987; 34(3): 371-406. DOI: 10.1080/09500348714550391.
[29] Sheppard CJR, Choudhury A. Annular pupils, radial polarization, and superresolution. Appl Opt 2004; 43(22): 4322-4327. DOI: 10.1364/AO.43.004322.
[30] Ratnam C, Lakshman Rao V, Goud SL. Comparison of PSF maxima and minima of multiple annuli coded aperture (MACA) and complementary multiple annuli coded aperture (CMACA) systems. J Phys D: Appl Phys 2006; 39: 4148-4152. DOI: 10.1088/0022-3727/39/19/005.
[31] Khonina SN, Ustinov AV, Pelevina EA. Analysis of wave aberration influence on reducing the focal spot size in a high-aperture focusing system. J Opt 2011; 13(9): 095702. DOI: 10.1088/2040-8978/13/9/095702.
[32] Khonina SN, Volotovskiy SG. Minimizing the bright/shadow focal spot size with controlled side-lobe in-crease in high-numerical-aperture focusing systems. Adv Opt Technol 2013; 2013: 267684. DOI: 10.1155/2013/267684.
[33] Araki T, Asakura T. Apodized images of coherently illuminated edges in the presence of defocusing and spherical aberration. Optika Aplicata 1978; VIII/4: 159-170.

Authors' information

Mekala Venkanna, Doctor of Physical Sciences; he works as Assistant Professor of Physics, Basic Sciences department, BVRIT Hyderabad College of Engineering for Women affiliated to Jawaharlal Nehru Technological University Hyderabad, India. Research interests: diffractive optics, coherent optical systems, spatial filters, image processing, meta materials. E-mail: *venkioptics@gmail.com*.

Karuna Dasari Sagar, Doctor of Physical Sciences; he works as a Professor of Physics and leader of Optics research group, Osmania Universty, Hyderabad, India. Research interests: Fourier optics, diffractive optics, spatial filters, image processing, photonics. E-mail: *dasari_ks@yahoo.com*.

Received June 16, 2021. The final version – December 16, 2021.